Research Article

Electric field induced patterning in Cr film under ambient conditions: A chemical reaction based perspective

Sumit Kumar[1] · Hasika Suresh[1] · Vijay A. Sethuraman[2] · Praveen Kumar[2] · Rudra Pratap[1]

Received: 29 July 2020 / Accepted: 29 October 2020

Abstract
Electric field-induced "etching" of Cr film is a tip-based patterning technique that is used to create micro- and nano-sized trenches in the film under ambient conditions. The experimental data obtained in this study reveals that the etching of Cr occurs *via* the formation of water-soluble CrO_3, which spontaneously forms at the cathode tip when a large electric field is applied using a pointed tip in the presence of humid air. By varying experimental conditions, such as vacuum level, gaseous environment, temperature, and humidity, the kinetics of the electric field induced chemical reaction at the cathode was studied. Subsequently, the obtained insights were incorporated into a model to explain the mechanism of the phenomenon. Water vapor in the air surrounding the tip acts as a limiting reactant in the electrochemical oxidation of Cr to CrO_3. Insights obtained from this study open new avenues for technological improvements in the patterning technique using this chemical method.

Keywords Cr film · Chemical reaction · Electric field-induced patterning · Electro-etching · Lithography under ambient conditions

1 Introduction

Scanning probe lithography (SPL) refers to a set of diverse patterning techniques involving modification of the substrate surface using a sharp tip. In practice, various types of SPL techniques have been invented depending on the nature of the interaction, such as mechanical, electrical, thermal, and chemical, between the tip and the substrate surface [1]. In particular, SPL techniques involving electric field or currents (SPL-E), such as electro-lithography (ELG) [2, 3], etc., are quite attractive, as they work under ambient conditions and produce patterns of widths ranging from a few nanometers to hundreds of micrometers using the same setup [3]. SPL-E may be implemented by a scanning tunneling microscope (STM), wherein a tunneling current can be used in the non-contact mode for oxidizing metals locally [4, 5], or an atomic force microscope (AFM), wherein a bias between the probe and the substrate is used to induce the desired surface modification, including oxidation, etc., in the contact mode [6]. Song et al. [4] demonstrated the formation of nanostructures in Cr film using STM under both low-dose (scanning mode) and high-dose (stationary) conditions. Similarly, Rolandi et al. [7] created 35 nm wide lines of MoO_3, with a pitch of 200 nm, by traversing an AFM tip on a 4 nm thick Mo film deposited on a p-type Si (100) substrate. In general, the rate of oxidation and the resolution of patterns depend on the electric field and the ambient conditions [8], and by optimizing them, various nanostructures, including quantum dots, point contacts and single-photon detectors, have been

Electronic supplementary material The online version of this article (https://doi.org/10.1007/s42452-020-03796-7) contains supplementary material, which is available to authorized users.

✉ Praveen Kumar, praveenk@iisc.ac.in | [1]Center for Nano-Science and Engineering, Indian Institute of Science, Bangalore, Karnataka 560012, India. [2]Department of Materials Engineering, Indian Institute of Science, Bangalore, Karnataka 560012, India.

Published online: 24 November 2020

created using SPL-E [9–11]. However, as explained next in the context of ELG, all SPL-E techniques suffer from lack of repeatability of patterns [2, 3, 9], that is often attributed to the lack of unambiguous understanding of the mechanism through which electric field or current interacts with the substrate surface. Resolving this ambiguity is the primary goal of this study.

ELG is a new SPL-E technique that is based on the electric current induced liquefaction of Cr film around the cathode tip [2, 3, 12]. As shown in Fig. 1a, application of an electric field between any two points in the Cr film using a pair of pointy electrodes leads to liquefaction of the material below the cathode, which then expands in radially symmetric fashion, thereby forming a circular liquefied flow-affected region, if the cathode tip is kept stationary. Now, as shown in Fig. 1b, if the cathode tip is traversed along a pre-set path while keeping the anode stationary, then a pattern is "electro-etched" in the Cr film. In practice, the material in the flow-affected region can be dissolved in water, thereby creating a trench into the Cr film. The trench pattern can then be transferred to another material using standard thin film deposition techniques or can be used as a mask for photolithography [3]. It should be noted that although the pattern shown in Fig. 1b has a width of ~100 µm, patterns as narrow as <10 nm in polymer and ~40 nm in transferred metal have been obtained using ELG [3]. Given the ease of operation of ELG, the faster rate of liquefaction of material and the excellent resolution of the patterns achieved by controlling the force applied onto the tip, electric field applied, etching of polymer layer placed in between Cr film and substrate, etc., ELG appears to be quite promising in terms of a unique combination of throughput and resolution [2, 3].

However, similar to other SPL-E techniques, there is a genuine scientific interest in understanding the mechanism of patterning by ELG, especially related to the role of chemical reaction in the surface modification and the identification of the compound formed in the flow-affected region. A study [6] has suggested CrO_3—a water-soluble, low melting temperature oxide of Cr—as the compound formed at the cathode tip in the Cr-film upon the application of an electric field through an AFM tip. However, while CrO_3 was identified as the compound formed through the STM-based technique also when the tip was kept stationary, the water-insoluble Cr_2O_3 with high melting temperature was suggested to form when the STM tip was traversing over the sample [4]. Furthermore, a previous study [3] reported the compound to be $Cr(NO_3)_3$, based on the energy dispersive spectroscopy (EDS) study performed inside a scanning electron microscope (SEM) and X-ray photo-spectrometry (XPS). However, these methods of material identification require the material to be exposed to a high vacuum, which may lead to a transformation of the weakly stable compound and hence the reaction product might have been misdiagnosed. Given the ambiguity in the identification of the reaction product formed at the cathode tip, it is imperative to carry out a detailed investigation of the electric current induced surface modification of Cr film. In this study, we have performed systematic experiments involving variation in the ambient conditions to identify the material formed in the flow-affected region near the cathode tip and to understand the kinetics of the chemical reaction taking place under the stationary tip condition. Consistent with an earlier study [6], the material in the flow-affected region was identified as CrO_3, which we report to form *via* electrolysis of water vapor present in the air. Although the results obtained in this study

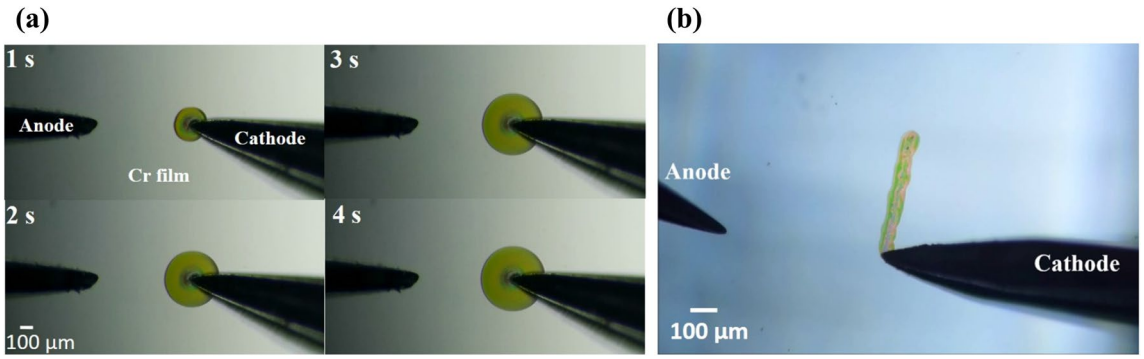

Fig. 1 Principle and working of ELG: (**a**) Time-lapse images showing various stages of growth of the circular flow-affected region around the cathode tip upon the application of a potential difference of 10 V across the two W-probe tips (see Supplemental Material 1 for a video of the process). The timestamp is given on the top-left region in each figure. (**b**) Pattern formation in Cr film deposited on Si substrate by traversing the cathode tip, while keeping the anode tip stationary (see Supplemental Material 2 for a video of the process)

are directly relevant to ELG (in the sense of usage of Cr film for patterning) and the stationary-tip condition, the results have been validated for the traversing-tip conditions also, and the implications will be relevant to other SPL-E techniques as well.

2 Experimental procedure

A 20–100 nm thick Cr film was deposited on SiO_2-Si substrate using direct current magnetron sputtering. The thin film sample was placed on the stage of a probe-station, and a constant potential difference, over a range of 10–20 V, was applied across two W-probes (see Fig. 2a for a schematic illustration as well as a picture of the setup). Herein, firstly the anode probe was brought into contact with the Cr film, and subsequently the cathode tip was slowly lowered down onto the same film. Once the cathode tip made contact with the Cr film, a sudden rise in the electric current, measured using a source measurement unit (SMU), was recorded. At the same time, material in the vicinity of the cathode tip alone liquefied, and the liquefied region grew away from the cathode tip in a radially symmetric fashion forming a circular flow-affected region (see Fig. 1a). The current (as well as voltage) profile was continuously recorded using the SMU, whereas the growth of the flow-affected region was continuously recorded using a digital camera: Both of these data were synchronized so that a correlation between the electric current (as well as the voltage) and the velocity at which the leading edge of the flow-affected region was expanding could be accurately established. The effect of experimental conditions, such as vacuum level, gaseous composition, substrate temperature, and humidity, was studied by placing the sample into a custom-built chamber, with provisions for attaching a vacuum pump, gas inlets (with a mass flow controller), electrical feed-throughs and a digital camera (see Fig. 2b for a picture of the setup).

Once a test was completed, the material from the flow-affected region was removed carefully by dissolving it in deionized (DI) water for a series of chemical analyses. A color-change based chemical analysis was performed to identify the chemical compound, wherein the extracted material was reacted sequentially with potassium hydroxide (KOH) and sulfuric acid (H_2SO_4), and the associated color change was observed. To further confirm the identity of the reaction product, fast Fourier infra-red (FTIR) spectroscopy was conducted under the ambient condition on the aqueous solution of the extracted material.

3 Results and discussion

3.1 Identification of reaction product

The color of the aqueous solution of the material extracted from the flow-affected region was orange, which matches with the color of the dichromate ($Cr_2O_7^{2-}$) aqueous solution [13]. In practice, the equilibrium shift test can be performed to verify the presence of dichromate ions: Here, the color change is observed upon mixing a small amount of acid and base to the sample [14]. When a small amount (*e.g.*, 1 ml, as used in this study) of a base (*e.g.*, KOH, as used in this study) was added to a 10 ml aqueous solution of the extracted material, its color changed from orange to yellow, which shows a shift in the equilibrium from the dichromate towards the chromate rich side. On the other hand, when a small amount (*e.g.*, 1 ml, asusedin this study) of a dilute acid (*e.g.*, H_2SO_4:$H_2O \equiv 1{:}3$, as used in this study) was added into the basic solution of the

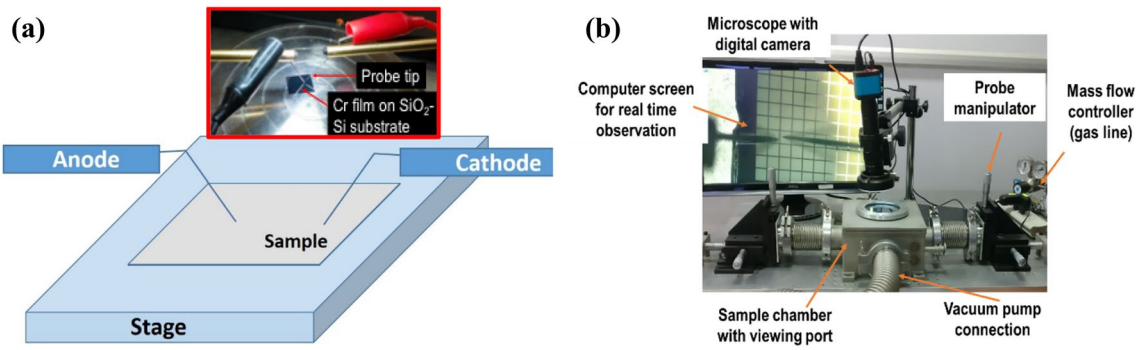

Fig. 2 (**a**) A schematic illustration of a sample-electrodes configuration in a probe-station. The inset on the top shows the digital photograph of the actual sample-electrodes configuration. (**b**) Digital picture of the custom-built test setup used to study the effect of the ambient condition on the electric current induced liquefaction and expansion of the flow-affected region in the Cr film. The picture in (**b**) also lists the major component of the setup

extracted material, it again became orange. This shows the equilibrium shift from chromate towards dichromate rich side [14]. Similar changes in color were observed for an aqueous solution of standard potassium dichromate ($K_2Cr_2O_7$) also. To further strengthen the conclusion of the presence of dichromate ions, 0.5 ml of H_2O_2 was mixed with 10 ml of the acidified solutions (H_2SO_4:$H_2O \equiv 1{:}3$) of both the material extracted from the flow-affected region and the standard $K_2Cr_2O_7$. For both materials, this H_2O_2 treatment resulted in the formation of a metastable deep blue color compound, which finally transformed into a light blue stable solution. This conclusively confirms similarity in the aqueous solutions of standard $K_2Cr_2O_7$ and the extracted material. Now, as it will be discussed later, the electric field induced liquefaction of Cr film was observed only in the presence of humid air, and hence the extracted material must be chromic acid (H_2CrO_4). Interestingly, the anhydride form of H_2CrO_4 is CrO_3, which appears to be the material formed in the flow-affected region. Similar observations were also noted for the material extracted from the liquefied region when the cathode tip was traversed (*i.e.*, when the tip was not static and it was under ELG mode).

Further conclusive chemical identification test was performed using FTIR spectroscopy, wherein the spectrum obtained from the aqueous solution of the extracted material was compared with that obtained from the aqueous solution of the high purity (99.99%) CrO_3 granules. Here, FTIR was performed under attenuated total reflection (ATR) mode. The scanning was repeated 32 times in the range 4000–500 cm^{-1}, and an average value was taken as the final spectrum. Deionized water acted as the background medium whose spectrum was subtracted from the spectra of both the solutions during the post-processing. Figure 3 shows the absorption spectra of the material extracted from the flow-affected region as well as the CrO_3 solution. Figure 3 clearly reveals a similarity in the spectra of both materials, with the wavenumber of the most intense peaks of the extracted material and the high purity CrO_3 granules to be equal to 947.77 cm^{-1} and 948.38 cm^{-1}, respectively. This peak position is attributed to the chromyl (*i.e.*, Cr = O) vibrations [15]. Hence, the color change based chemical tests and the FTIR spectroscopy conclusively confirm that the material formed in the flow-affected region, *i.e.*, at the cathode, due to the application of an electric current through Cr film, was CrO_3.

3.2 Liquid form of reaction product

One of the consistent observations related to the application of electric current is the liquefaction of material in the flow-affected region near the cathode, *i.e.*, the new material formed below the cathode remained in a liquid state, giving an impression that a "flow-affected region" has formed due to application of the electric field. Since the melting temperature of oxides is generally very high (*e.g.*, CrO_3 melts at 197 °C), this observation requires further examination. It should be noted that the role of Joule heating might be limited here as a high resolution (better than 0.25 K) infra-red based thermal camera did not pick up any change in the temperature of the material near the cathode during the formation and the liquefaction of the reaction product. Interestingly, CrO_3 is hygroscopic, with an acidic aqueous form. Consistently, the pH values of the high and low concentration aqueous solutions of the reaction product were measured to be 0.7 and 2.88, respectively. The hygroscopic nature of the reaction product was verified by performing thermal cycling and vacuum tests. The Cr sample after the formation of the reaction product was heated to 45 °C by placing it on a hot-plate. The liquid portion of the reaction product disappeared upon

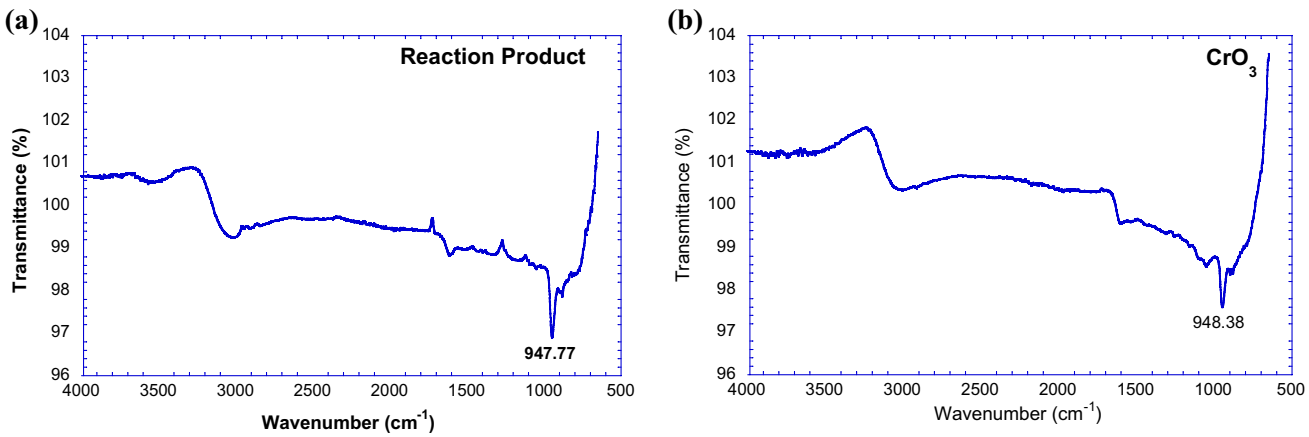

Fig. 3 FTIR spectra of the aqueous solutions of the (**a**) material extracted from the flow-affected region (termed as *Ring material* here) and (**b**) high purity CrO_3 granules. The wavenumber of the prominent peak in each spectrum is highlighted

heating, leaving behind only a solid residue. Interestingly, when the sample was cooled back to 25 °C, the solid residue again became liquid. Furthermore, when the Cr film sample comprising the reaction product was placed inside the vacuum chamber, the reaction product remained in the liquid form at a pressure of 900 mbar, and it started to solidify at pressures of <100 mbar. Interestingly, when the chamber was vented (thereby increasing the pressure), the solidified reaction product became liquid again. Since a part of the water evaporates (and hence leaves the vacuum chamber), transforming the remaining water into ice at high vacuum [16], this reversible transformation in the state of the reaction product can be attributed to the corresponding transformation between solid and liquid states of water at high and low vacuum, respectively, and trapping of the water vapor from the air at higher pressures. These two tests suggest that the reaction product remains liquid under ambient condition due to extremely fast absorption of the water vapor from the air by it, and not due to heating above the melting temperature.

3.3 Reaction current

Figure 4 is a representative graph showing the variation of the reaction current, as measured using an SMU, and areal velocity (i.e., the rate of change of the area) of the flow-affected region, as measured using the video showing the expansion of the flow-affected region at the cathode, as functions of time. It should be noted that the electric current passing through the sample in the absence of the chemical reaction was negligible, and hence the current profile shown in Fig. 4a is attributed to the current generated due to the chemical reaction. As shown in Fig. 4a, the reaction current, and hence the rate of chemical reaction, at first increased rapidly to a maximum value and then decreased slowly to a very small

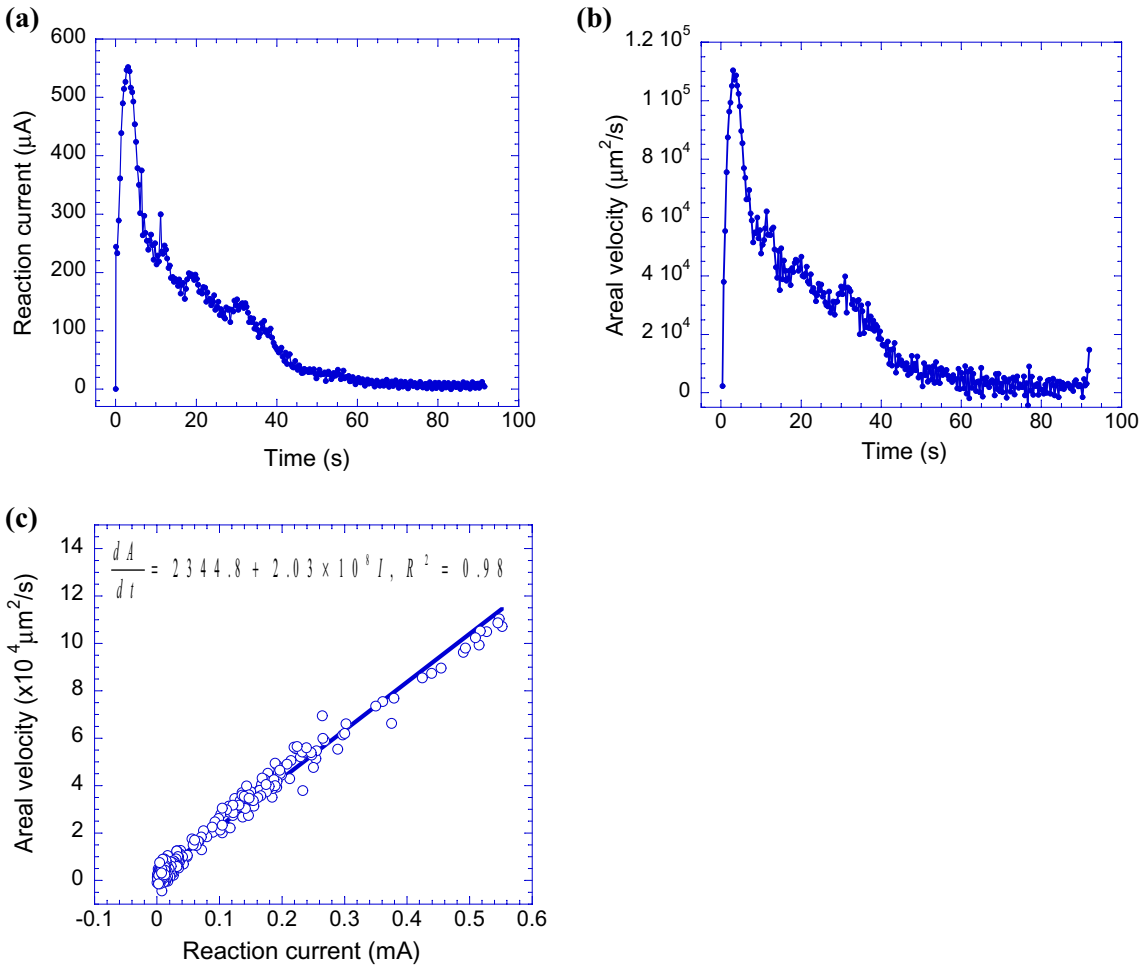

Fig. 4 Variation of (**a**) reaction current and (**b**) areal velocity of the flow-affected region with time. (**c**) Variation of the areal velocity of the flow-affected region as a function of the reaction current. In (**c**), the solid line passing through the datum points represents the best fit linear curve whose equation, along with the regression parameter (R^2), are given in the legend. The thickness of Cr film was 100 nm and a potential difference of 10 V was applied between the two probes

value with time. The peak reaction current, presumably due to transport limitations of one of the reactants, can be assumed to correspond to the maximum rate of the chemical reaction. A comparison of Fig. 4a, b reveals that the areal velocity profile matches with the reaction current profile, suggesting that the reaction current is indeed an excellent measure of the rate of the chemical reaction in these tests. This correspondence was further confirmed by plotting the areal velocity with respect to the reaction current (see Fig. 4c). The linear relation between the areal velocity and the reaction current, as shown in Fig. 4c, indicates the Faradaic nature of the chemical reaction at any instant during the reaction [17]; this will be discussed further in Sect. 3.5.

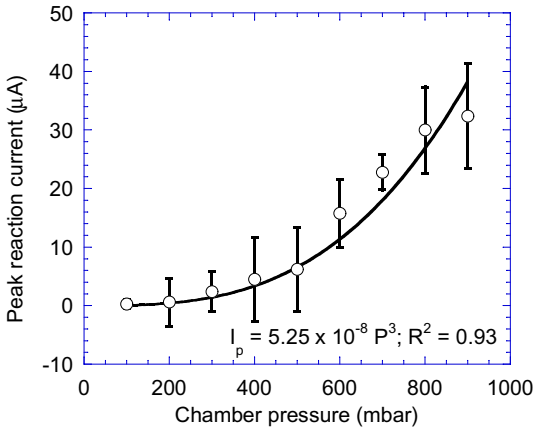

Fig. 5 Variation of the peak reaction current as a function of the pressure inside the chamber. The solid curve shows the best fit curve, whose equation is also given in the legend. The symbols and the error bar correspond to the mean and the standard deviation of datum points, respectively. The thickness of the Cr film was 10 nm and a potential difference of 10 V was applied between the two electrodes while performing this set of experiments

3.4 Effect of ambient conditions on electric field-induced chemical reaction

Figure 5 shows the effect of the chamber pressure on the peak reaction current. It should be noted that the chemical reaction was not observed at the chamber pressure of ≤1 mbar. This can be attributed to the unavailability of the reactants (*e.g.*, as it will be shown later, H_2O in the air). Furthermore, continuous chemical reaction, leading to the formation of the circular liquefied region (akin to a ring around the electrode tip), whose diameter could be measured unambiguously, and the generation of the reaction current beyond the resolution of the SMU, could not be observed up to a chamber pressure of 200 mbar. As shown in Fig. 5, when the chamber pressure was increased above 200 mbar (and up to 900 mbar), then the peak reaction current increased cubically with the chamber pressure.

The absence of the chemical reaction, and hence the non-existence of the consequent liquefied flow-affected region, at a high vacuum level, and a rather exponential decrease in the reaction current with time, lead to the following question: "If air flows directly onto the reaction site, then would the decaying reaction current profile exhibit an increase?" Herein, while the reaction product was forming at the cathode tip, an air blower was used to flow the air directly onto the sample at a very high rate. As shown in Fig. 6, the reaction rate was dramatically enhanced as the air-flow was directed on the cathode probe. This increased rate of reaction was reflected in the higher current peak in

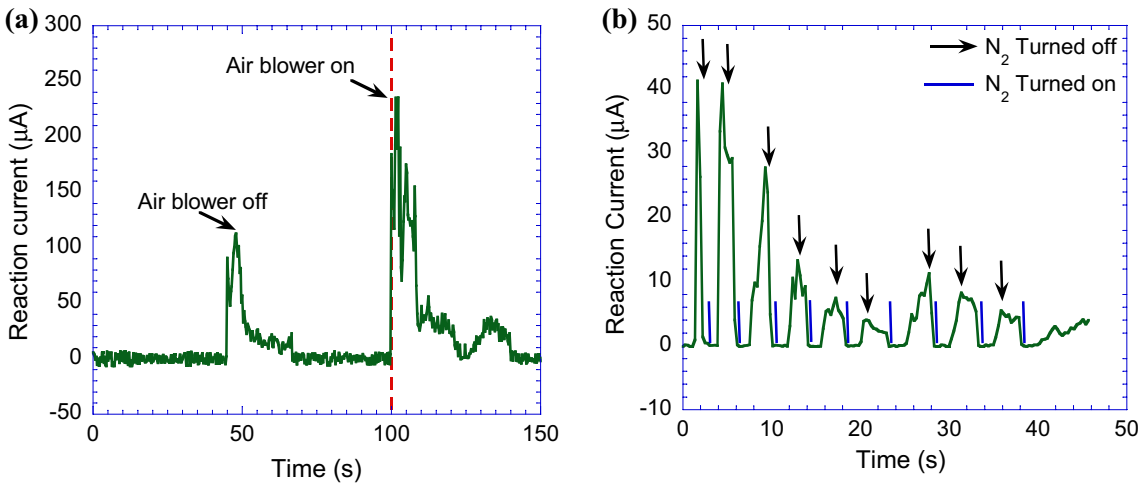

Fig. 6 Effect of the blowing (**a**) air and (**b**) N_2 at the reaction site on the variation of the peak reaction current as a function of time. The vertical line in (**a**) marks the instant at which the air blowing started. In (**b**), N_2 was blown in steps of 2 s, and each event of turn-on and turn-off of N_2 gas is marked by an arrow and a line, respectively

comparison to the peak current observed for the reaction occurring without the air-flow.

Similarly, when N_2 or O_2 gas was flown directly over the reaction site in the sample, then the chemical reaction inhibited completely, and simultaneously the reaction current decreased to a very small value (*e.g.*, in the range below the resolution limit of SMU)—see Fig. 6b. A decrease in the reaction current upon passage of N_2 clearly suggests that N_2 not only does not participate in the chemical reaction, but it also displaces the reactants away from the reaction site. Interestingly, as shown in Fig. 6b, when the flow of N_2 was stopped, the chemical reaction at the cathode started again, which was reflected by a simultaneous increase in the reaction current and the diameter of the flow-affected region. The peak current decreased with time, as was also evident in the chemical reaction occurring in the normal environment (see Fig. 4). However, the reaction current was still significant even after 40 s of the start of the experiment. This high peak current after long-duration suggests that the flowing N_2 removed the air deficient in reactants and allowed replenishment of the same with new air, which had a better proportion of the reactants (*e.g.*, water vapor in the form of humidity, as will be discussed later).

This set of experiments clearly shows that some constituents of the ambient air are the major reactants in the chemical reaction occurring at the cathode. However, it is important to identify the actual reactant(s). Therefore, experiments were repeated inside a vacuum chamber in O_2 and N_2 environments. However, the chemical reaction was neither observed in O_2 nor N_2 environment. Experiments were repeated even in the combined $O_2 + N_2$ environment, wherein they were mixed in different ratios. However, here also chemical reaction did not occur. Furthermore, the chemical reaction did not occur in dry air (*i.e.*, zero humidity), which clearly reveals the important role of humidity in controlling the chemical reaction in Cr film at the cathode. To further confirm this inference, a petri dish filled with water was kept inside the vacuum chamber over a hot-plate. Subsequently, vacuum pumps were turned on, creating a high vacuum inside the chamber. At this point, the residual water in the petri dish was converted into ice, and the chemical reaction was not observed. Now, as the heater (attached to the hot-plate) was switched on, the water started to boil, and the pressure in the vacuum chamber increased due to the water vapor. Subsequently, the heater was switched off, and the water was left for 2–3 h over the hot-plate to cool down, which resulted in heavy humidification of the chamber. Subsequently, a potential difference of 10 V was applied across the two probes touching the Cr-film and, quite interestingly, the chemical reaction initiated at a significantly faster rate as compared to the rates observed under standard air environment. Subsequently, the same process was repeated in the humidified gaseous environment: Herein, at first, the vacuum chamber was filled with either O_2 or N_2 or their mixtures up to 700 mbar, and then water vapor was "added" by heating the water placed in the petri dish, as before. In all such test conditions, the chemical reaction was observed unambiguously. This set of observations conclusively indicates that humidity is solely responsible for the chemical reaction observed in Cr film at the cathode.

To further understand the critical role of the water vapor or the humidity in the chemical reaction in Cr film at the cathode, the effect of sample temperature on the reaction kinetics was studied. Here, a 20 nm Cr film sample was kept on the hot-plate, and the electric current was passed at different temperatures. The temperature of the hot plate was increased from room temperature (*ca.* 25 °C) to 75 °C in steps of 5 °C. As shown in Fig. 7, the diameter of the flow-affected region decreased with the temperature of the hot plate. The chemical reaction responsible for the formation of the flow-affected region was not observed above 60 °C. The decreased kinetics of the reaction with an increase in the temperature can be attributed to the loss of the water vapor from the sample surface. A careful observation of Fig. 7 reveals that the diameter of the flow-affected region decreased exponentially with the sample temperature, T. Now, the coefficient of $1/T$ in the best curve-fit equation can be related to the enthalpy of water evaporation. As water molecules adsorbed on the sample surface are responsible for the chemical reaction, the following may be written:

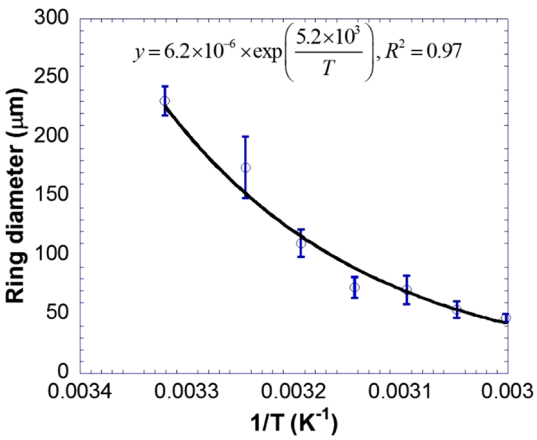

Fig. 7 Variation of the diameter of the liquefied flow-affected region as a function of the hot-plate temperature. The solid line shows the exponential curve fit, whose equation and the curve fitting regression parameter (R^2) are shown in the legend. The symbols and the error bar correspond to the mean and the standard deviation of the datum points, respectively

$$\dot{m}_{rxn} \propto \frac{1}{W_v} \cong \exp\left(\frac{\Delta H_v}{RT}\right) \quad (1)$$

where $\dot{m}_{rxn}$ is the rate of formation of the reaction product, W_v is the rate of evaporation of the water, ΔH_v is the enthalpy of evaporation and R is the universal gas constant. Now, comparing the exponential term in Eq. (1) and the coefficient of 1/T in Fig. 7 gives 46.6 kJ/mol as the value of enthalpy of water evaporation, which is close to the actual value of enthalpy of water evaporation (*i.e.*, 40.8 kJ/mol). These observations and calculations further confirm that water (as humidity) is the major reactant in the chemical reaction occurring at the cathode.

3.5 Rate controlling chemical reaction mechanism

Based on the results presented in the previous sub-sections, the following three aspects about the chemical reaction occurring in Cr can be deduced: (1) reaction occurs only at the cathode, (2) the reaction product is CrO_3, and (3) humidity and hence water vapor is one of the reactants, besides Cr. Based on these three observations, the chemical reaction at the cathode can be given as follows [1, 18]:

$$Cr + 3H_2O \xrightarrow{e^-} CrO_3 + 6H^+ + 6e^- \quad (2)$$

The above chemical reaction equation can now be used to establish a quantitative relation between the amount of the reaction product and the current measured during the chemical reaction.

A mathematical relationship between the areal velocity and the reaction current can be derived from the Faraday's relation. Current, I, flowing during the electrochemical reaction can be expressed as [17]:

$$I = nF\frac{dM_p}{dt} \quad (3)$$

where n is the number of electrons or charge transferred during the chemical reaction, F is Faraday constant, M_p is the number of moles of the product formed, and t is the time. M_p can be written in terms of the area of the rings, as follows:

$$M_p = \frac{m}{M} = \frac{\rho h A_{rxn}}{M} \quad (4)$$

where m is the mass of the reaction product and M is the molecular mass of the reaction product. Now, m can be given as the product of the density, ρ, and the volume of the reaction product, which can be given as the product of the area of the reaction product, A_{rxn}, and its height, h. Therefore, assuming h to remain constant throughout the process, the areal velocity of the ring formation can be determined by inserting Eq. (4) into Eq. (3):

$$\frac{dA_{rxn}}{dt} = \frac{M}{nF\rho h} I \ \mu m^2/s \quad (5)$$

Equation (5) predicts a linear relationship between the areal velocity and the reaction current, which is consistent with the variation observed experimentally (see Fig. 4c). Now, taking the values of ρ and M to be 2.7 g/cm^3 and 100 g/mol, respectively, for CrO_3 and n to be equal to 6 (see Eq. (2)), one can calculate the value of h to be equal to 319 nm for the reaction product in the flow-affected region formed in the 100 nm thick Cr film sample (see Fig. 4c for relevant data on dA_{rxn}/dt). This value is, indeed, of the same order as the thickness of the reaction product (300–500 nm) formed in the 100 nm thick Cr film. It should be noted that the thickness of the reaction product in the flow-affected region was non-uniform, and its average thickness varied with the thickness of the as-deposited Cr film. For example, the thickness varied between 100 and 200 nm in the 20 nm thick Cr films. Hence, the above match between the prediction and the experimental data (within the scatter of the data) confirms the efficacy of Eq. (2) in representing the chemical reaction occurring in Cr at the cathode.

Now, the rate of the chemical reaction (Eq. 2) can be written in terms of the concentration of the reactants as follows:

$$R_{rxn} = [Cr]_s \left[H_2O\right]^3_{vap} \quad (6)$$

where R_{rxn} is the rate of the reaction. $[Cr]_s$ can be taken as unity (because the reactant is in solid form), and $[H_2O]_{vap}$ can be assumed to scale with the partial pressure of water vapor in the air and hence the pressure itself. Accordingly, the reaction rate can be written in terms of the partial pressure of the water vapor, as follows:

$$R_{rxn} = kP^3_{H_2O} = k' P^3 \quad (7)$$

where P represents the chamber pressure for the reactions performed inside the vacuum chamber. Now, the reaction current reflects the rate of the reaction, and hence it can be expected to follow the relationship:

$$I \propto R_{rxn} \propto P^3 \quad (8)$$

Interestingly, the experimental data shown in Fig. 5a suggests:

$$I_{peak} \propto P^3 \quad (9)$$

which is consistent with Eq. (8) indicating that the reaction order is indeed three and that the limiting reactant is

water. It should be noted that although Eq. (9) represents a relation between for the maximum (or peak) current and the pressure, the theoretical prediction of the reaction current variation with pressure (*i.e.*, Eq. (8)) can be considered consistent with the experimental data as the peak current is the characteristic of the reactants of the chemical reaction, and their transport properties. The gradual drop in the reaction current (see Fig. 4) and a sudden rise in the reaction current upon "blowing" the reactants at the reaction site (see Fig. 6a) suggest that the chemical reaction here is diffusion-controlled, wherein the reaction rate gradually decreased due to the lack of one of the reactants (*i.e.*, H_2O) because of the slow migration of the reactants from the air nearby to the reaction site. In this scenario, the peak current represents the stage of the reaction where the chemical reaction is expected to follow Eq. (7) most ideally. Hence, the peak current, which is also the most easily identifiable parameter in the reaction current profile, can be considered as the characteristic of the chemical reaction. Overall, the experimental observations quantitatively match with the chemical reaction outlined in Eq. (2), thereby confirming it to be the chemistry of the phenomenon of the electric current induced chemical reaction in Cr.

4 Conclusion

Electric field-induced patterning in Cr film, as in electrolithography (ELG), occurs due to the phenomenon of electric field-induced chemical reaction at the cathode. Water vapor in air dissociates and provides reaction species to form hygroscopic CrO_3, which remains liquefied throughout the reaction process.

Variations of the reaction current and the rate of expansion of the reaction products reveal the Faradaic nature of the chemical reaction. The kinetics of the chemical reaction, measured in terms of the radius of the flow-affected region at the cathode and the reaction current, increases rapidly with the air pressure. A power-law relationship between the chamber pressure and the reaction current, with an exponent of 3, is observed.

Faster metal etching rates, and hence enhancement in the throughput for electrolithography, can be attained by increasing the humidity. Slow etching rate, which is essential for obtaining patterns with high resolution, is possible either in a less humid environment or at low pressures.

Acknowledgments The authors would like to acknowledge the financial support provided by DSTO 1526 (Technology System Development Program of Department of Science and Technology, India) and DSTO 1759 (Indo-Russia Joint Research Project of Program of Department of Science and Technology, India). We are thankful to Professor Navakanta Bhat of Indian Institute of Science, Bangalore, for providing his lab facilities for a specific work.

Compliance with ethical standards

Conflict of interest On behalf of all authors, the corresponding author states that there is no conflict of interest.

References

1. Garcia R, Martinez V, Martinez J (2006) Nano-chemistry and scanning probe nanolithographies. Chem Soc Rev 35:29–38
2. Kumar S, Abraham E, Talukder S, Kumar P, Pratap R (2018) Micro electrolithography system development. In: 4th IEEE international conference on emerging electronics (ICEE). IEEE, New York, pp 1–4
3. Talukder S, Kumar P, Pratap R (2015) Electrolithography—a new and versatile process for nano patterning. Sci Rep 5:1–11
4. Song HJ et al (1994) 25 nm chromium oxide lines by scanning tunnelling lithography in air. J Vacuum Sci Technol B Microelectron Nanometer Struct 12:3720–3724
5. Xie W, Dai X, Xu LS, Allee DA, Spector J (1997) Fabrication of Cr nanostructures with the scanning tunnelling microscope. Nanotechnology 8:88–93
6. Wang D, Tsau L, Wang KL, Chow P (1995) Nanofabrication of thin chromium film deposited on Si(100) surfaces by tip induced anodization in atomic force microscopy. Appl Phys Lett 67:1295–1297
7. Rolandi M, Quate FC, Dai H (2002) A new scanning probe lithography scheme with a novel metal resist. Adv Mater 14:191–194
8. Avouris P, Marte R, Hertel T, Sandstrom R (1998) AFM-tip-induced and current-induced local oxidation of silicon and metals. Appl Phys A Mater Sci Process 66:659–667
9. Garcia R, Knoll AW, Riedo E (2014) Advanced scanning probe lithography. Nat Nanotechnol 9:577–587
10. Puddy RK, Chua CJ, Buitelaar MR (2013) Transport spectroscopy of a graphene quantum dot fabricated by atomic force microscope nanolithography. Appl Phys Lett 103:183117–183121
11. Pannetier B, Villegier J, Bouchiat V (2012) Quantum and thermal phase slips in superconducting niobium nitride (nbn) ultrathin crystalline nanowire: application to single photon detection. Nano Lett 12:3501–3506
12. Talukder S, Kumar P, Pratap R (2013) Electric current-induced mass flow in very thin infinite metallic films. IEEE Trans Electron Devices 60:2877–2883
13. Rao GG (1966) Potassium dichromate as an oxidimetric reagent. Talanta 13:1473–1495
14. Weckhuysen BM, Wachs IE, Schoonheydt RA (1996) Surface chemistry and spectroscopy of chromium in inorganic oxides. Chem Rev 96:3327–3349
15. Trivedi MK et al (2015) Powder metallurgy & mining characterization of physical, thermal and structural properties of chromium(VI)oxide powder: impact of biofield treatment. J Powder Metall Min 4:1–4
16. Shin HT, Lee YP, Jurng J (2000) Spherical-shaped ice particle production by spraying water in a vacuum chamber. Appl Therm Eng 20:439–454
17. Zanello P, de Biani FF, Nervi C (2003) Inorganic electrochemistry: theory, practice, and application. Royal Society of Chemistry, Cambridge
18. Sugimura H, Uchida T, Kitamura N, Masuhara H (1994) Scanning tunneling microscope tip-induced anodization for nanofabrication of titanium. J Phys Chem 98:4352–4357